

Annual Review of Marine Science

A Synoptic View of the Ventilation and Circulation of Antarctic Bottom Water from Chlorofluorocarbons and Natural Tracers

Sarah G. Purkey,¹ William M. Smethie Jr.,²
Geoffrey Gebbie,³ Arnold L. Gordon,²
Rolf E. Sonnerup,^{4,5} Mark J. Warner,⁶
and John L. Bullister⁵

¹Scripps Institution of Oceanography, University of California, San Diego, La Jolla, California 92093, USA; email: spurkey@ucsd.edu

²Lamont-Doherty Earth Observatory, Columbia University, Palisades, New York 10964, USA; email: agordon@ldeo.columbia.edu, bsmeth@ldeo.columbia.edu

³Department of Physical Oceanography, Woods Hole Oceanographic Institution, Woods Hole, Massachusetts 02543, USA; email: ggebbie@whoi.edu

⁴Joint Institute for the Study of the Atmosphere and Ocean, University of Washington, Seattle, Washington 98195, USA; email: rolf@uw.edu

⁵Pacific Marine and Environmental Laboratory, National Oceanic and Atmospheric Administration, Seattle, Washington 98115, USA; email: john.l.bullister@noaa.gov

⁶School of Oceanography, University of Washington, Seattle, Washington 98195, USA; email: warner@u.washington.edu

**ANNUAL
REVIEWS Further**

Click here to view this article's online features:

- Download figures as PPT slides
- Navigate linked references
- Download citations
- Explore related articles
- Search keywords

Annu. Rev. Mar. Sci. 2018. 10:503–27

First published as a Review in Advance on September 6, 2017

The *Annual Review of Marine Science* is online at marine.annualreviews.org

<https://doi.org/10.1146/annurev-marine-121916-063414>

Copyright © 2018 by Annual Reviews.
All rights reserved

Keywords

Antarctic Bottom Water, chlorofluorocarbons, deep-ocean ventilation, abyssal warming, bottom limb of the meridional overturning circulation, changes in ocean circulation

Abstract

Antarctic Bottom Water (AABW) is the coldest, densest, most prolific water mass in the global ocean. AABW forms at several distinct regions along the Antarctic coast and feeds into the bottom limb of the meridional overturning

circulation, filling most of the global deep ocean. AABW has warmed, freshened, and declined in volume around the globe in recent decades, which has implications for the global heat and sea level rise budgets. Over the past three decades, the use of tracers, especially time-varying tracers such as chlorofluorocarbons, has been essential to our understanding of the formation, circulation, and variability of AABW. Here, we review three decades of temperature, salinity, and tracer data and analysis that have led to our current knowledge of AABW and how the southern component of deep-ocean ventilation is changing with time.

1. INTRODUCTION

As early as the *Challenger* expedition of 1872–1876, deep waters of the global ocean have been traced back to an Antarctic source (Sverdrup et al. 1942). Now known as Antarctic Bottom Water (AABW), this water mass occupies the largest volume of any water mass in the ocean. AABW circulates from its formation sites around Antarctica throughout the global ocean as part of the bottom limb of the meridional overturning circulation (MOC) and may be isolated from the surface for a millennium or longer. In recent decades, AABW has warmed, freshened, and decreased in volume (Purkey & Johnson 2010, 2012, 2013), suggesting a large-scale shift in Southern Ocean deep ventilation.

AABW is produced primarily in three locations along the Antarctic continental shelf (Orsi et al. 1999) (**Figure 1**). At each formation site, a pool of cold, dense shelf water forms through complex interactions with the continental shelf below, the ice shelf above, and the atmosphere when katabatic winds open coastal polynyas (Foster & Carmack 1976, Rintoul 1998, Gordon 2013) (**Figure 2**; see also Section 2). Within polynyas, the surface waters are able to exchange gases and approach equilibrium with the atmosphere (Schlosser et al. 1991, Rodehacke et al. 2009). As the dense water circulates under the ice shelf, it interacts with the ice shelf through melting and freezing (Jacobs 2004), gaining an isotopic signature from glacial ice meltwater and the release of gases trapped in glacial ice bubbles (e.g., Schlosser et al. 1991). Finally, as the shelf water flows across the shelf break and down the continental slope, it entrains ambient waters, primarily modified Circumpolar Deep Water (CDW), to produce AABW.

Direct observation of AABW formation is challenging owing to the relatively small spatial and temporal scales of dense-water formation events and the inhospitable environments near formation sites. The tagging of AABW with chemical signatures from contact with the atmosphere, glacial ice, and the unique biological characteristics of the shelf formation regions has been a key tool in advancing our understanding of the production, circulation, and volume of AABW flowing from source regions to the global ocean through the bottom limb of the MOC.

Here, we review the use of anthropogenic transient tracer gases—chlorofluorocarbons (CFCs) and sulfur hexafluoride (SF_6)—and natural tracers in advancing our understanding of AABW and its variability. We start by describing where and how AABW forms around Antarctica (Section 2) and review the use of tracers to estimate deep-ocean ventilation rates (Section 3). In Section 4, we discuss specifically how tracers have been used to quantify AABW formation rates and circulation. Finally, we shift away from the steady-state assumption and present temperature, salinity, and CFC data that support the growing evidence that AABW properties and volume are changing (Section 5). We conclude with a brief discussion of future applications of CFCs and SF_6 that could improve our understanding of the processes driving the continuing variability in AABW formation and circulation.

AABW: Antarctic Bottom Water

MOC: meridional overturning circulation

CDW: Circumpolar Deep Water

CFC: chlorofluorocarbon

SF₆: sulfur hexafluoride

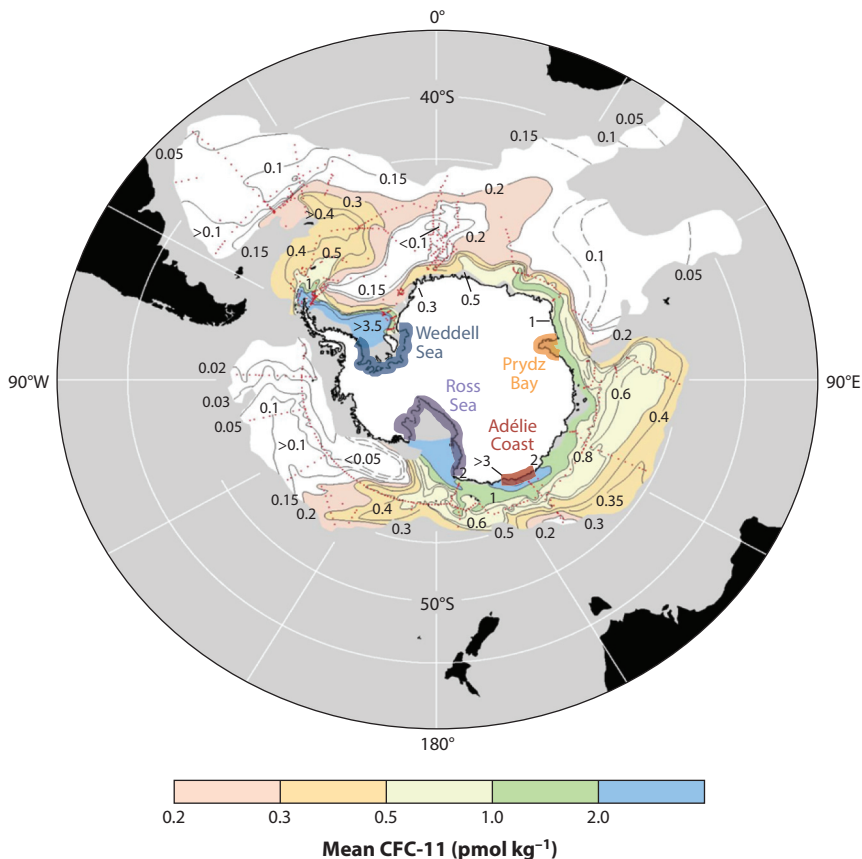


Figure 1

Mean concentrations of the chlorofluorocarbon CFC-11 (CCl_3F) within the Antarctic Bottom Water layer (defined as bottom waters with a neutral density greater than 28.27 kg m^{-3}) from data (red dots) collected either before or during the World Ocean Circulation Experiment (WOCE). The four regions of AABW formation—the Weddell Sea, the Ross Sea, the Adélie Coast, and Prydz Bay—are highlighted. Adapted from Orsi et al. (1999) with permission from Elsevier.

2. CONTINENTAL MARGIN BOTTOM WATERS, OPEN OCEAN CONVECTION, AND THE SEASONALITY OF DENSE-SHELF-WATER EXPORT

Dense water forms on the Antarctic continental shelf as cold polar air spreads seaward, extracting heat from the coastal waters. The resultant cooling and salinification, via sea-ice production, form dense shelf water (Jacobs et al. 1985) that is eventually exported in thin ($<400 \text{ m}$) descending plumes over the continental slope into the deep ocean as AABW, cooling the lowest kilometer of the world ocean (Legg et al. 2009, Gordon 2013, Heywood et al. 2014).

Antarctica is not zonally symmetric: Along the 18,000-km Antarctic margin are sectors of narrow and wide continental shelves. There are also regions where the margins recede poleward, forming the large embayments of the Weddell and Ross Seas, or protrude northward, such as the margins of East Antarctica and the Antarctic Peninsula. Additionally, the distance between the continental margin and the warm deep waters of the Antarctic Circumpolar Current varies,

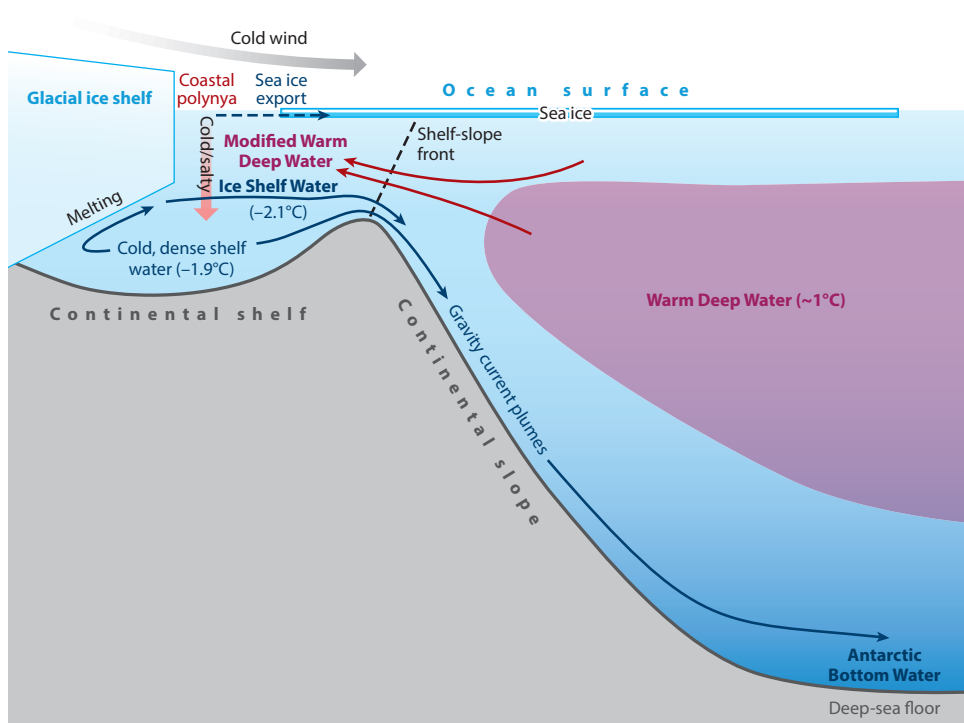


Figure 2

Schematic of Antarctic Bottom Water formation along the Antarctic continental shelf and slope. Cold shelf water forms through brine rejection in coastal polynyas during ice formation and export. The shelf water flows down the slope in dense plumes, mixing with ambient Warm Deep Water (also referred to as modified Circumpolar Deep Water). Potential temperatures pertinent to Weddell Sea Bottom Water formation are also shown. Adapted from Gordon (2013) with permission from Elsevier.

from the close approach in the southeast Pacific sector to the greater separation offshore of the Weddell Sea, affecting the properties of the shelf water. As a consequence of the air-sea fluxes and the properties of the regional shelf/slope water type exchange, the shelf water of the Antarctic margin varies in temperature and salinity, producing a range of AABW varieties (Gordon 1974).

The Weddell and Ross Seas are the primary sites of export of dense shelf water, while sites along the Antarctic margins south of Australia and within the Indian Ocean sector contribute less (Jacobs et al. 1970; Gordon 1974, 2013; Foster & Carmack 1976; Baines & Condie 1998; Gebbie & Huybers 2011; Ohshima et al. 2013; Heywood et al. 2014) (**Figure 1**). The AABW produced in the Weddell Sea [Weddell Sea Bottom Water (WSBW)] has a characteristic potential temperature of -1.0°C and a salinity of 34.64; the Ross Sea produces the saltiest AABW [Ross Sea Bottom Water (RSBW)], with a characteristic potential temperature of -0.8°C and a salinity of 34.70 (Jacobs & Comiso 1989; Gordon et al. 2010, 2015). The characteristics of the AABW produced in the Australian and Indian Ocean sectors are closer to those of the WSBW, although the production rates are lower. The transport of WSBW off the shelf is approximately 4–5 sverdrups (Sv) ($1 \text{ Sv} = 10^6 \text{ m}^3 \text{ s}^{-1}$), apparently drawing from a shelf water flux of 1–3 Sv (Gordon 1998; Fahrbach et al. 1995; Gordon et al. 1993, 2010). The production of AABW from the Ross Sea reaches the deep ocean along two paths: $\sim 1.7 \text{ Sv}$ as a boundary current off Cape Adare, drawing High-Salinity Shelf Water (HSSW) from the western Ross Sea, and lower-salinity bottom water

WSBW: Weddell Sea Bottom Water

RSBW: Ross Sea Bottom Water

Sv: sverdrup ($1 \text{ Sv} = 10^6 \text{ m}^3 \text{ s}^{-1}$)

HSSW: High-Salinity Shelf Water

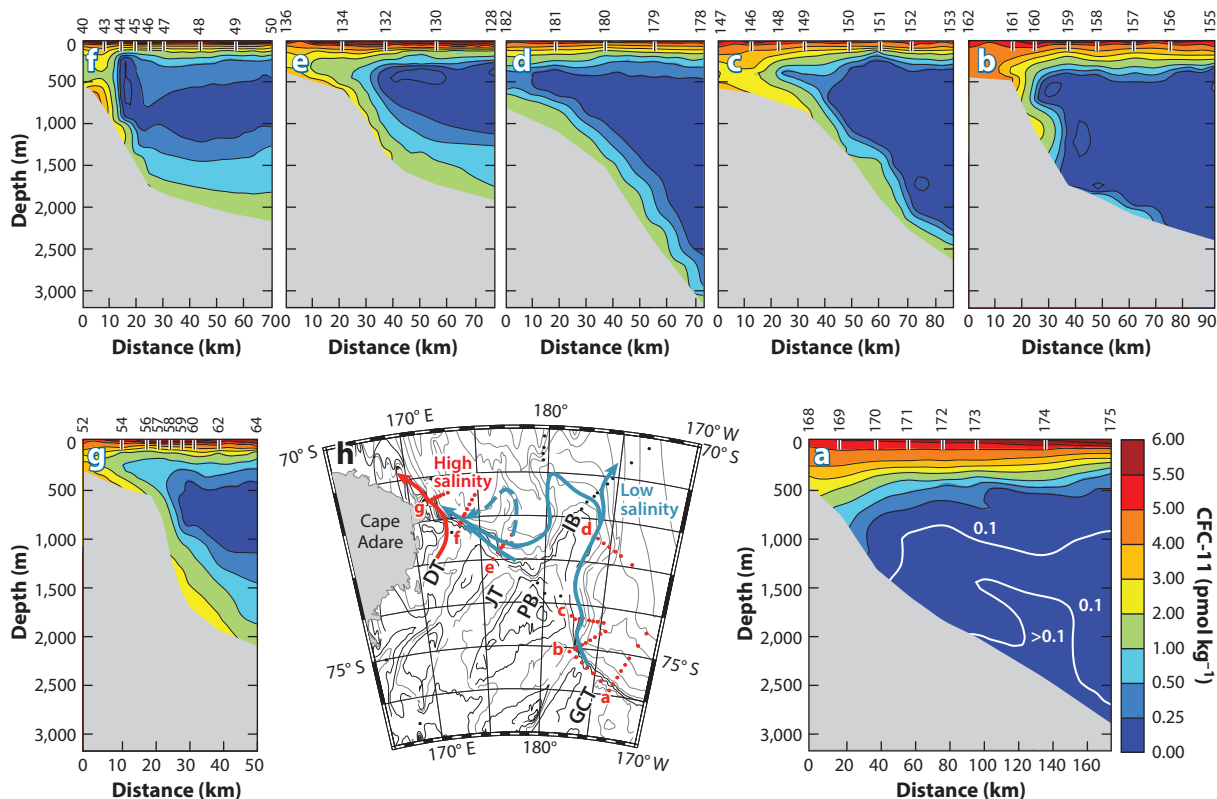


Figure 3

Cross-slope transects of the chlorofluorocarbon CFC-11 (CCl_3F) along the Ross Shelf break during AnSlope II in February–April 2004. Red dots denote the station locations corresponding to tick marks and numbers above panels *a–g*. The sections start to the east (panel *a*) and move counterclockwise around the shelf to the west (panel *g*); panel *b* shows the locations of the sections along the shelf break. Panel *b* also shows the pathways of the low-salinity (blue) and high-salinity (red) shelf waters from the primary deep troughs (DT, Drygalski Trough; JT, Joides Trough; GCT, Glomar Challenger Trough), following figure 1 from Gordon et al. (2009). Pennell Bank (PB) and Iselin Bank (IB) are also labeled for reference.

drawn from the central Ross Sea and exported east of Iselin Bank (Gordon et al. 2004, 2009, 2015; Orsi & Wiederwohl 2009) (**Figure 3**). The AABW contribution from east of Iselin Bank is not well determined; some may flow into the Cape Adare bottom current, but some enters the southeast Pacific basin (Gordon 1966). AABW formed in the Cape Darnley Polynya of the Indian Ocean sector of Antarctica, to the west of Prydz Bay and the Amery Ice Shelf, contributes approximately 0.7–1.5 Sv of AABW (Ohshima et al. 2013). The direct contribution from Prydz Bay is not clearly determined (Yabuki et al. 2006). Bottom water formed along the Adélie Coast (Gordon & Tchernia 1972) has also not been fully quantified but may be significant (Rintoul 1998, Williams et al. 2008).

Winter coastal polynyas—strips of near-zero sea-ice cover along the Antarctic coast—are important regions for the formation of dense shelf waters (**Figures 1 and 2**). Within coastal polynyas, enormous quantities of sea ice form as cold, dry air spreads seaward over the ocean. The sea ice is subsequently blown northward (offshore), maintaining the coastal polynya, enabling more ice to form, and boosting the salinity and density of the (near-freezing) water column. Thus, the coastal polynyas act as sea-ice factories. Nihashi & Ohshima (2015) identified 13 Antarctic coastal

polynyas, the largest of which are the Mertz Polynya in the Australian sector of Antarctica, the Ross Ice Shelf and Terra Nova Bay Polynyas of the Ross Sea, and the Cape Darnley Polynya of the Prydz Bay region of the Indian Ocean sector. These large, wind-forced coastal polynyas appear in roughly the same location every winter and allow for the renewal of local shelf water. A large coastal polynya also forms in the Weddell Sea (Paul et al. 2015).

At some of these sites, such as the Weddell and Ross Seas, the shelf water is made even colder from contact with the northern face and base of extensive floating glacial ice shelves, leading to the formation of Ice Shelf Water (ISW) as cold as -2.3°C , well below the freezing point of seawater at the ocean surface. The cold ISW chills the shelf water, making it more susceptible to sinking to the deep-sea floor owing to the greater compressibility of colder water (the thermobaric effect).

CFC concentrations indicate that the total export of Antarctic shelf water is approximately 5.4 Sv, which upon entrainment of deep water forms 17.5 Sv of AABW (Orsi et al. 2001, 2002). The western Ross Sea, the formation site for a particularly salty variety of AABW (Gordon 1974, Jacobs et al. 1985, Orsi & Wiederwohl 2009), accounts for approximately 25% of AABW formation (Orsi et al. 2002) (for further discussion, see Section 4.2).

In addition to the dense water formed along the margins of Antarctica, deep-reaching open ocean convection occurs in the Weddell Sea. During the austral winters of 1974–1976, near 66°S and the Greenwich meridian, a large region normally covered by winter sea ice remained ice free throughout the winter, referred to as the Weddell Polynya (Gordon 1978, 2014; Gordon et al. 2007). During the Weddell Polynya episode, the normal stratification changed as cold surface water sank to depths of 3,000 m. During the three winters of the persistent Weddell Polynya, 1–3 Sv of surface water entered the deep ocean. What triggered the Weddell Polynya is unclear, although it may have resulted from a prolonged negative phase of the Southern Annular Mode (Gordon et al. 2007). Model simulations of the Weddell Polynya suggest that it was a response to strengthening of westerly winds (Cheon et al. 2015) and that the ocean convection and cooling of the deep water affected the waters of the Weddell Sea continental margin (Wang et al. 2017).

The export of shelf water to the deep ocean depends on the position of the shelf-slope front that separates the shelf regime from the deep open ocean. The AABW derived from the Weddell Sea displays a seasonal cycle in bottom temperatures, with a cold pulse in May or June and a warm pulse in October or November. The timing and intensity of these phases vary each year (Gordon et al. 2010). Seasonal fluctuations of WSBW properties are likely governed by the seasonal cycle of the winds over the western margin of the Weddell Sea, with the interannual variability reflecting the Southern Annular Mode and El Niño/Southern Oscillation (Gordon et al. 2010, McKee et al. 2011). The shelf-slope front moves seaward during the weaker winds of the austral summer, allowing the shelf waters of the southwestern Weddell Sea to spill into the deep ocean in late-summer months. This is consistent with the model results of Stewart & Thompson (2012, 2013, 2015) and the overview by Heywood et al. (2014). Increased winds parallel to the continental shelf break shift the dense shelf water toward the coast, inhibiting the export of shelf water into the deep ocean, whereas the weaker winds of summer allow the shelf water to spread seaward, feeding plumes descending the continental slope. In this way, the export of shelf water into the AABW realm depends not only on the air-sea buoyancy flux, but also on the circulation induced by the wind momentum flux.

A 2007–2010 time series off Cape Adare revealed a similar seasonality of AABW export from the Ross Sea (Gordon et al. 2009, 2015). The maximum bottom speeds at the time of the coldest and saltiest events mark an export of the HSSW from the western Ross Sea in late austral summer, similar to the Weddell Sea. A secondary cold bottom water event that is not coupled to high salinity occurs in October and November, suggesting that lower-salinity Ross Sea shelf water originates from the Glomar Challenger Basin to the east of Pennell Bank (**Figure 3**). Williams

et al. (2008) reported similar seasonality and interannual variability in the export of dense water from the Adélie Depression into the Australian-Antarctic Basin.

3. TRACERS QUANTIFY DEEP-OCEAN VENTILATION AND CIRCULATION

During the past six decades, anthropogenic substances have been produced that have proven to be excellent tracers for ocean ventilation, including bomb tritium and its daughter product from radioactive decay, ^3He ; bomb radiocarbon; CFCs; and SF_6 . These substances are often referred to as transient tracers because their input to the ocean varies with time (Figure 4). Because their input histories to the sea surface can be reconstructed and they are conservative in the ocean interior, these tracers provide quantitative information about ocean ventilation timescales.

The utility of transient tracers for investigating ocean circulation and ventilation was first realized in the 1970s following observations of bomb tritium and radiocarbon, produced by atmospheric nuclear weapons testing, in the deep North Atlantic during the Geochemical Ocean Sections Study (GEOSECS) program (Broecker & Peng 1982). In the early 1980s, oceanic CFC

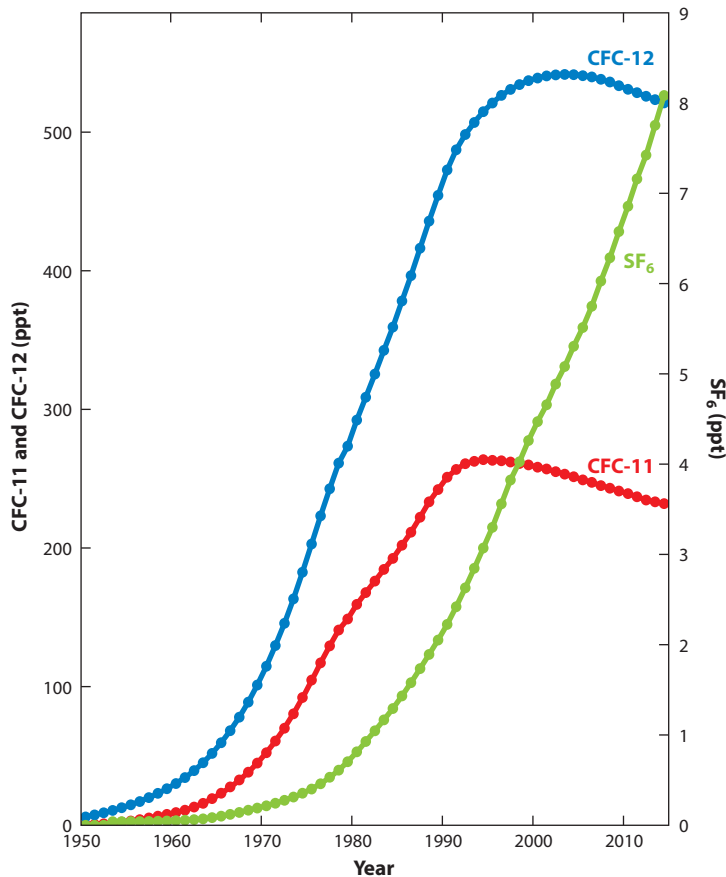


Figure 4

Atmospheric history of the chlorofluorocarbons CFC-11 (CCl_3F) and CFC-12 (CCl_2F_2) and sulfur hexafluoride (SF_6) in parts per trillion (ppt). Data are from Bullister (2015).

WOCE: World Ocean Circulation Experiment

CLIVAR: Climate Variability and Predictability

GO-SHIP: Global Ocean Ship-Based Hydrographic Investigations Program

GLODAPv2: Global Ocean Data Analysis Project version 2

measurements revealed high concentrations of CFC-11 (CCl_3F) and CFC-12 (CCl_2F_2) in the deep Nordic Seas (Bullister & Weiss 1983), the deep North Atlantic (e.g., Weiss et al. 1985, Fine & Molinari 1988, Pickart et al. 1989, Smethie 1993), and the deep Southern Ocean adjacent to the Antarctic continent (e.g., Bullister 1989, Trumbore et al. 1991). We focus here on the use of CFCs to trace AABW production.

Production of CFC-12, used extensively in refrigeration and air conditioning, began in the 1930s, and production of CFC-11, used as an aerosol spray propellant, as an expansion gas in plastic foams, and in many manufacturing processes, began in the 1940s; the production of both increased significantly in the 1950s, and their concentrations in the atmosphere increased rapidly until 1990 (Bullister 2015) (**Figure 4**). Because they catalyze stratospheric ozone destruction and are powerful greenhouse gases, the atmospheric time histories of both gases are carefully monitored with a global network for trace gas measurements [the Advanced Global Atmospheric Gases Experiment (AGAGE) (<https://agage.mit.edu>) and the National Oceanic and Atmospheric Administration's Earth System Research Laboratory (<https://www.esrl.noaa.gov>)]. Restrictions on production of CFC-11 and CFC-12 were initiated in the late 1980s, and their atmospheric concentrations are now slowly decreasing (**Figure 4**). They continue to enter the ocean interior as surface water is converted to denser subsurface water and will continue to propagate into the deep-ocean interior on timescales from decades to centuries because of their slow decrease ($\sim 1\%$ per year) in the atmosphere. SF_6 , which is used extensively as an electrical insulator in high-voltage equipment, began entering the atmosphere, and hence the oceans, in significant quantities approximately two decades later than CFCs (**Figure 4**). Its concentration has been increasing monotonically since the 1960s and nearly linearly since the mid-1980s and is monitored by the same networks used to monitor CFCs. CFCs and SF_6 can be measured onboard ship during research cruises, and their measurement has become standard in many oceanographic studies.

Hundreds of thousands of dissolved CFC measurements have been made in the ocean. The World Ocean Circulation Experiment (WOCE), Climate Variability and Predictability (CLIVAR) repeat hydrography, and the Global Ocean Ship-Based Hydrographic Investigations Program (GO-SHIP) provided quasi-synoptic coverage of all of the ocean basins and repeat occupations every 5–10 years of basin-wide sections with high-quality temperature, salinity, oxygen, nutrient, and transient tracer (CFCs, SF_6 , tritium, ^3He , and ^{14}C) data (Talley et al. 2016). The WOCE program ended in the late 1990s, but the GO-SHIP program reoccupies a portion of the WOCE sections, documenting changes in the world ocean as the climate warms. Many other programs focusing on smaller regions or specific oceanographic processes have also been carried out with extensive tracer measurements. Many of these data are included in the Global Ocean Data Analysis Project version 2 (GLODAPv2) data compilation (Olsen et al. 2016).

3.1. Chlorofluorocarbons in Deep Circulation Pathways

The distributions of CFCs and SF_6 clearly reveal deep circulation pathways. Because these compounds have existed for only a few decades, their presence reveals flow paths that have existed during this time period. They also provide quantitative information on the rate of subsurface water formation and the transport times of the deep flow.

Formation rates can be calculated from CFC inventories. The CFC inventory of a subsurface water mass directly reflects its formation rate over the time of CFC input to the formation region. The source water CFC concentration as a function of time can be calculated from the well-known atmospheric time history (**Figure 4**) and used to calculate the rate of input of source water needed to match the observed total inventory (e.g., Orsi et al. 1999, Smethie & Fine 2001, Rhein et al. 2002, LeBel et al. 2008). Repeating the calculation over different time intervals can

reveal temporal variability in the formation rate. This method has three potentially significant sources of uncertainty: (a) inaccuracy in determining the total CFC inventory within a water mass owing to the lack of synoptic coverage of CFC measurements on basin to ocean-wide scales; (b) uncertainty in the source water concentration because equilibrium of the source water with the well-known atmospheric concentration is not always achieved, especially in regions of rapid deep convection and ice cover where dense water is produced; and (c) uncertainty from assuming a constant formation rate over the time of tracer input.

Deepwater transport times can be determined in two ways: (a) fitting circulation models to the observed CFC (or SF₆) concentration and (b) determining transit times for water to flow from the source region to the point of observation (also referred to as age or isolation time from the surface) by comparing the observed CFC (or SF₆) concentration with the time history of concentration in the source water (e.g., Fine et al. 2003). The most straightforward way to do the latter is to calculate the gaseous partial pressure of the CFC (*p*CFC) from the dissolved CFC concentration using its solubility, a function of temperature and salinity (Warner & Weiss 1985), and then compare this value with the atmospheric time history (**Figure 4**) to determine the date of formation (e.g., Doney & Bullister 1992). This can also be done using tracer ratios such as CFC-11:CFC-12 if the ratio has varied with time (e.g., Smethie et al. 2000). The *p*CFC method yields an accurate mean age if no mixing with water parcels of different ages has occurred; if mixing has occurred, it still can do so when the change in CFC input has been linear during the time of input. For the situation where mixing with old tracer-free water occurs, the ratio method yields the mean age of the youngest component of the mixture. In reality, a water parcel is typically a mixture of components with different ages. The transit time distribution (TTD) technique takes mixing into account and provides information on both the mean age and age distribution of a water parcel (e.g., Waugh et al. 2004, Steinfeldt et al. 2009, Holzer et al. 2010). When used with a single tracer, assumptions must be made about the ratio of mixing to advection, but this can be constrained by using a suite of tracers with different input functions. The method can be applied to nonsynoptic data, assuming the circulation field is in a steady state. It can also be used to investigate variability in circulation by applying it to observations repeated in time, such as GO-SHIP repeats of WOCE sections.

4. TRACING ANTARCTIC BOTTOM WATER AROUND THE WORLD

The extensive oceanic measurements of CFCs over the past 35 years have revealed in striking detail how AABW forms and spreads throughout the global ocean. Here, we review key findings of the past four decades.

4.1. Quantifying Antarctic Bottom Water Formation Rates Using Tracers

Time-varying atmospheric gases and the ratios of the stable gas isotopes from glacial meltwater have been used to trace and quantify AABW formation at and directly downstream from AABW formation sites. In high-latitude regions, glaciers are enriched in certain stable isotopes and transfer that isotopic signature into ISW through glacial water addition during melting processes beneath the ice shelf (Weiss et al. 1979, Schlosser 1986, Schlosser et al. 1991, Huhn et al. 2008) (**Figure 2**).

In the Weddell Sea, CFCs and the isotopes of noble gases have been used to identify AABW production in and around the Filchner Depression and Larsen C ice shelf. Schlosser et al. (1990) found that ISW in front of the Filchner Depression contained 1.4% pure glacial melt and demonstrated that these isotopic signatures could be used to trace ISW out of Filchner Depression and into WSBW. Following this work, Weppernig et al. (1996) estimated that WSBW contained 15% ISW, with a formation rate of 5 Sv. Mensch et al. (1996) estimated that at least 3.5 Sv of WSBW

was being produced in this region, for a total addition of 11 Sv of AABW, using a kinematic box model fit to the hydrographic and CFC data. Farther to the west, Huhn et al. (2008) used helium and neon isotopes to show that an additional ~ 1 Sv of deep water was being formed in front of the Larsen C ice shelf, which contained 0.1% pure glacial meltwater. Furthermore, CFC analysis revealed a roughly 5-year residence time on the shelf and a 9-year mean transit time between the western source and the bottom water at 0°E (Mensch et al. 1996, Huhn et al. 2008).

In the eastern Ross Sea, Low-Salinity Shelf Water has high CFC concentrations and an age of approximately 2.5 years, indicating recent ventilation, whereas the fresher ISW found on the central shelf has lower CFC concentrations, with tracer ages of approximately 4 years (Trumbore et al. 1991). These CFC concentrations suggest that the time for transforming HSSW to ISW under the ice ranges from 4.1 to 4.8 years (Smethie & Jacobs 2005), or from 5.5 to 7.5 years if corrections for dilution from low-CFC CDW are applied (Loose et al. 2009). As HSSW transitions to ISW, it travels under the glacial ice shelf and gains fresh water, and this freshening is reflected in its isotopic composition. Using helium, neon, and $\delta^{18}\text{O}$, Loose et al. (2009) showed that the newly formed ISW gained 8% fresh water from pure glacial melt.

CFCs have been used in both the Ross and Weddell Seas to trace dense plumes of high-CFC shelf water off the shelf and into the deep currents along the continental slope (e.g., Mensch et al. 1996). **Figure 3** shows CFC-11 cross sections of the continental slope in front of the Ross Shelf measured as part of the AnSlope program. These cross sections clearly show the newly formed AABW cascading down continental slopes and feeding the along-slope current, supporting earlier analyses of AABW formation and circulation proposed by Gordon et al. (2009) (**Figure 2**). Water travels west along the continental slope, following the bathymetry around the Ross Shelf. The section shown in **Figure 3a**, located farthest to the east, shows almost no CFCs along the upper slope, indicating little or no deepwater ventilation here, but there is a small signal along the lower slope that may have been advected from the Weddell Sea. By the section shown in **Figure 3c**, however, a young high-CFC plume at 1,000 m has entered the slope current from the Glomar Challenger Trough (**Figure 3b**). As the plume travels north along the east side of the Ross Shelf, its CFC concentration decreases, indicating mixing with low-CFC CDW, but it is still present to the northern edge of Iselin Bank (**Figure 3d**). On the west side of the Ross Shelf, newly ventilated shelf water with high CFC concentrations again enters the along-slope current upstream of the section shown in **Figure 3e** and of the section shown in **Figure 3g**, indicating shelf water plumes from the Joides and Drygalski Troughs, respectively.

Similar cross-slope CFC surveys were conducted along the Adélie–George V Coast, revealing a similar dual deepwater production on either side of Mertz Bank (Williams et al. 2010). Bottom CFC concentrations (figure 16 in Williams et al. 2010) along with potential temperature–salinity properties show newly ventilated low- and high-salinity deep water from the Mertz Sill and Adélie Sill, respectively, suggesting a similar ISW formation process for the Ross Sea, albeit with a different seasonal cycle (Williams et al. 2010).

4.2. Chlorofluorocarbons in the Deep Southern Ocean

The first global analysis of CFCs in AABW was conducted using data collected before and during WOCE (Orsi et al. 1999). The mean concentrations of CFC-11 within the AABW layer, defined as all bottom waters with a neutral density greater than 28.27 kg m^{-3} , clearly show the formation and outflow from the Ross Sea, Weddell Sea, and Adélie Coast (Orsi et al. 1999) (**Figure 1**). The highest mean CFC concentrations are directly off and west of the Weddell Shelf, highlighting the importance of these formation regions. From here, the CFCs follow the flow around the Weddell Gyre and exit to the north into the Atlantic. In the Indo-Pacific sector, CFC distributions suggest

that AABW originates from the Ross Shelf and Adélie Coast. AABW from both of these regions enters the coastal current and is carried quickly westward, confined tightly to the continental slope, resulting in very young high-CFC waters all along the Indian Ocean sector of the Antarctic Slope as far east as the Princess Elizabeth Trough. AABW from the coastal current leaks into the Australian-Antarctic Basin, keeping this deep basin relatively well ventilated. CFC concentrations in the bottom waters of the Australian-Antarctic Basin adjacent to the continental slope are highest at 140°E and lower to both the east and west, consistent with the input of recently ventilated waters from the Adélie–George V Coast (Williams et al. 2010). In the South Pacific, the deep CFCs suggest recent ventilation into and around the Ross Gyre. Low CFC values to the east in the Bellingshausen Basin, however, indicate that RSBW is slow to cross the dynamical eastern gyre boundary, causing this to be the least well-ventilated of the deep Southern Ocean basins. The total inventory of CFCs in the AABW layer from the WOCE observations, using the inventory technique described above, indicates a total AABW production rate in the range of 8.1–9.4 Sv, with the Atlantic, Pacific, and Indian Ocean sectors responsible for 61%, 22%, and 17%, respectively (Orsi et al. 1999, 2002).

Regional studies of CFCs in the Southern Ocean and beyond complement the global analysis of Orsi et al. (1999). Haine et al. (1998) used CFC concentrations along hydrographic sections between the Weddell Sea and Australian-Antarctic Basin with a simple plume model to estimate 0.8–1.6 Sv of eastward-flowing Weddell Sea Deep Water (WSDW) and WSBW into the abyssal South Indian Ocean. Meredith et al. (2001) used a one-dimensional advection-diffusion model to estimate a stronger transport of 3.2 Sv into the Indian Ocean and an additional 0.9 Sv into the South Atlantic through the Vema Channel, implying a total of 3.7 Sv of deep and bottom water production in the Weddell Sea. Assuming a steady circulation, Klatt et al. (2002) used CFCs from multiple occupations of the Greenwich meridian section across the Weddell Sea to calculate the relative contributions of shelf water, shelf saturation levels, and transit time to the section of all water masses. They found that WSBW had a transit time of 13.5 ± 2.5 years and concluded that there had been no significant change in the ventilation rate between 1984 and 1998. Even at the northern end of the AABW's pathway, the absence of CFCs in AABW underlying the higher-CFC North Atlantic Deep Water was used to measure mixing and flow near the end of its pathway as it travels north into the Guiana Basin (Rhein et al. 1998).

4.3. The Evolution of CFC-11 in the Antarctic Bottom Water Layer

Here, we attempt to visualize the temporal spread of CFC-11 into AABW by extending Orsi et al.'s (1999) work centered between 1987 and 1993 to the present. We use all data points in the GLODAPv2 data set (Olsen et al. 2016) that self-report a neutral density greater than 28.27 kg m^{-3} . The 8,812 data points from 1983 through 2011 that meet this neutral density criterion are binned on the $0.5^\circ \times 0.5^\circ$ horizontal-resolution grid of the WOCE Global Hydrographic Climatology (Gouretski & Koltermann 2004), and the mean value in the AABW layer is calculated by averaging all data points over a given calendar year. The mean and its error are calculated under the simplifying assumptions that the data are independent and that there are no sampling biases of the bottom layer, although these assumptions are not strictly true because the AABW layer is sometimes sampled by only one or two bottles.

Most grid points on the $0.5^\circ \times 0.5^\circ$ spatial grid have data for no more than 3 calendar years over the 29-year interval of interest. For any given year, however, CFC-11 data collected in previous and future years are valuable and can be used to constrain the deep flow of AABW. Orsi et al. (1999), for example, used a time-correction method to produce one map with data from different years (**Figure 1**). Here, we extend this procedure to time correct all data for 1983–2011, creating

a time-correction method that leverages knowledge of the atmospheric CFC-11 history. At each location, a least squares problem is solved for a TTD that fits the existing GLODAPv2 data within its uncertainty when convolved with the atmospheric history. The TTD is assumed to be steady through time, but no structure is assumed for its shape. Given the small number of data points in time relative to the number of unknowns in the TTD (~65 values, one for each year from 1948 to 2012), the problem is highly underdetermined. To produce a unique solution, we use a nonnegative weighted least squares method that forces the TTD to be strictly positive and as temporally smooth as possible. In recognition that significant uncertainties may remain, we also produce a formal error estimate of the CFC-11 concentration through time. This method is advantageous in that the estimated oceanic CFC-11 concentration is implicitly constrained to follow the atmospheric trend.

After using the time-correction method, we have time series of CFC-11 concentration at 1,162 of the 23,863 spatial grid points on the WOCE Global Hydrographic Climatology grid. To fill in the spatial map, we take the CFC-11 data and its uncertainty arising from averaging and time correction and use a two-dimensional objective mapping method (Bretherton et al. 1976). Following Orsi et al. (1999), we use an 850-km length scale in the zonal direction and a 350-km length scale in the meridional direction. We can then create an objective map and its error for each year from 1983 to 2011 by repeating the process with the appropriately modified error statistics on the data (**Figure 5**).

Figure 5 shows the time evolution of CFC-11 into the AABW layer of the Southern Ocean from 1985 to 2010 with the associated error. The time evolution animates the arrival of CFCs throughout the deep Southern Ocean. The Atlantic sector of the 1987 map (**Figure 5b**) and the Indo-Pacific sector of the 1993 map (**Figure 5d**) are directly comparable to the Atlantic and Indo-Pacific sectors of **Figure 1**, respectively. Note that a first-order difference is that Orsi et al. (1999) took knowledge of the bottom circulation and properties into account to guide the mapping of **Figure 1**, whereas we followed exactly the procedure described above based on the CFC data alone. Where they differ primarily reflects how each method accounts for regions with few data. In addition, objective mapping can create false maxima in extrapolation regions; however, these regions are collocated with high error and should not be considered robust (**Figure 5i**). **Figure 5i** shows the objective mapping error for 2010, which closely reflects the mapping error for 1985–2005 (not shown).

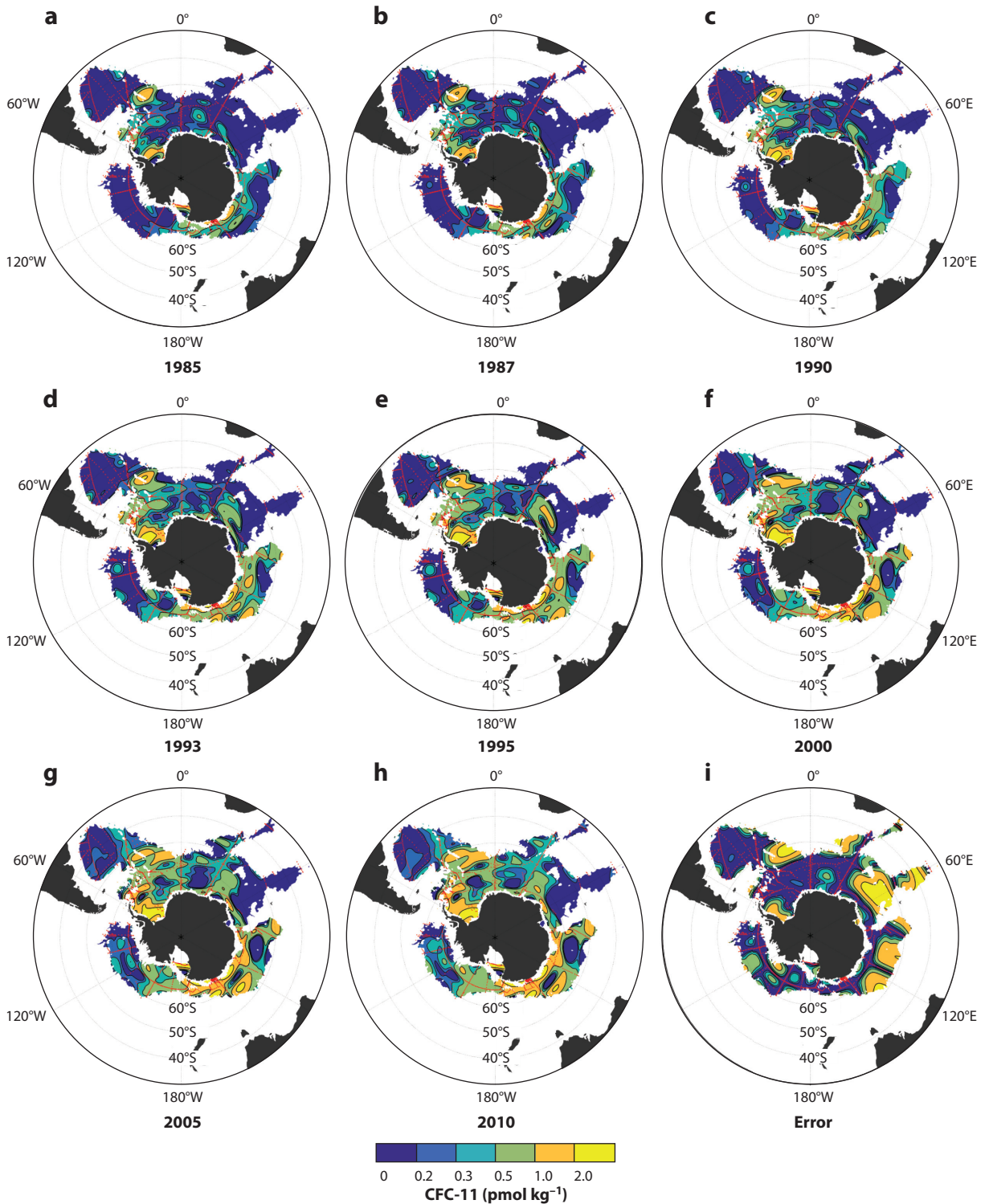
The annually mapped CFCs will allow for future evaluation of the time-changing AABW circulation. Despite the underdetermined nature of the problem, the GLODAPv2 data are not fit within their uncertainty in many locations, pointing to the expected limits of the steady-state assumption for the TTDs. Similarly, Huhn et al. (2013) showed that the TTD was changing with time within the Weddell Gyre (see Section 5). Further quantification of the TTD fit is needed along individual sections to quantify the exact circulation slowdown required to fit the data.

4.4. Transient Tracers in Antarctic Bottom Water Beyond the Southern Ocean

Since WOCE, CLIVAR and GO-SHIP repeat sections have monitored the arrival of CFCs beyond the Southern Ocean and as far north as the equator (**Figure 6**). The arrival of CFCs to

Figure 5

Objective maps of the mean concentrations of the chlorofluorocarbon CFC-11 (CCl_3F) within the Antarctic Bottom Water layer (defined as bottom waters with a neutral density greater than 28.27 kg m^{-3}) using a time-corrected method to project all available CFC-11 data (*red dots*) from 1985 (panel *a*) through 2010 (panel *b*) along with error (panel *i*). (For a description of the method used to create these maps, see Section 4.3.)



DWBC: deep western boundary current

the north highlights the deep circulation pathways, provides information on AABW transit times, and provides estimates of the rates of storage of anthropogenic carbon in the deep ocean.

The 2009–2011 occupations of the zonal GO-SHIP repeat hydrography sections along 32°S highlight the importance of the deep western boundary current (DWBC) in transporting AABW northward (**Figure 6a,b**). Here, AABW is less dense (neutral density of $\sim 28.2 \text{ kg m}^{-3}$) than the pure AABW found in the Southern Ocean owing to mixing with overlying waters. At 32°S, the highest concentrations of CFCs ($> 0.15 \text{ pmol kg}^{-1}$) are within the northward-flowing WSBW in the South Atlantic's DWBC around 45°W. In the West Indian Ocean, also fed by WSBW, high CFC concentrations are present in the DWBC along the Mozambique Escarpment and across the Mozambique Basin at 40°E. In addition, high CFC concentrations are present on either side of the Southwest Indian Ridge at 55°E extending above 3,000 m, indicating local enhanced vertical mixing owing to rapid bottom flow over rough topography. The deep eastern Indian Ocean basins filled with AABW from the Indo-Pacific have only trace levels of CFCs, however, indicating slower ventilation and older AABW. This is consistent with the long pathway AABW must take around the rim of the Australian-Antarctic Basin and across the Southeast Indian Ridge before entering the South Australian Basin (van Wijk & Rintoul 2014).

The Pacific DWBC flows northward along the southwest Pacific basin and through the Samoan Passage and is a major source of waters ventilating the deep central and North Pacific basins (**Figure 6a**). AABW in this DWBC has a lower maximum CFC compared with its Atlantic and Indian Ocean counterparts, reflecting a greater influence of Lower CDW owing to a higher sill depth entering the basin and possibly a longer transit time from source regions (van Wijk & Rintoul 2014) (**Figure 6a**). A model study indicated that more than half of AABW enters the subtropical oceans via this northward transport just east of New Zealand (Van Sebille et al. 2013). Abyssal CFC maxima have been observed in this DWBC on several WOCE/CLIVAR/GO-SHIP sections throughout the southwest Pacific basin and north through the Samoan Passage.

In particular, the meridional P15S section along 170°W intersects this DWBC in several locations, and P15 reoccupations illustrate the progress of the CFC transient in the abyssal subtropical southwest Pacific and its arrival in the tropical Pacific (**Figure 6c–f**). CFCs along P15 have been easily measurable at the seafloor since the 1990s (**Figure 6d**). Although low in concentration, CFCs clearly delineate the pathways of the ventilated component of the deep and bottom waters toward and through the Samoan Passage at 9°S. At the same time, CFC levels in the middle of the water column (1,500–3,500 m) remain below detection over much of the P15S section, providing an important opportunity to confidently determine CFC analytical blanks, a necessary step in correcting the measured CFCs to compute transports in the abyssal southwest Pacific to good precision. The P15S sections repeated in time capture the northward penetration of CFCs from the Southern Ocean to approximately 9°S in 1996 (**Figure 6d**) and to the equator in 2009 (**Figure 6e**). The Samoan Passage CFC signal, only a few hundred meters thick in 1996, was approximately 800 m thick in 2009, and CFCs were detectable over the bottom 1,300 m in 2016.

These CFC observations can be related to the transport of other anthropogenic perturbations, such as CO₂ and heat, in the southwest Pacific DWBC using methods applied previously in the North Atlantic (Pickart et al. 1989, Doney & Jenkins 1994, Waugh & Hall 2005) and the South

Figure 6

(a,b) Depth distributions of the chlorofluorocarbon CFC-11 (CCl₃F) measured along 32°S from the 2011 occupation of line A10, 2009 occupation of line I05, and 2009 occupation of line P06 (panel a) along with track locations (panel b). (c–f) Time evolution of the chlorofluorocarbon CFC-12 (CCl₂F₂) along line P15S in the South Pacific ($\sim 170^\circ\text{W}$; panel c) in 1996, 2009, and 2016 (panels d, e, and f, respectively).

Indian Ocean (Haine et al. 1998). Although these simple variants of pipe models overlook details of the abyssal transport, they do provide a means of estimating the appropriate time lag of arrival and transport of long-term anthropogenic anomalies from the high-signal-to-noise analogues (CFCs, SF₆, and CCl₄) that are readily measurable in the DWBC. For illustration, a 1.5-dimensional model (Waugh & Hall 2005), tuned to available CFC observations in the DWBC and Samoa Passage, indicates an anthropogenic *p*CO₂ increase in the Samoan Passage of 2.12 ppm in 2009. Using the dissolved inorganic carbon and alkalinity measured in the Samoan Passage during 2009, this *p*CO₂ increase translates to an anthropogenic dissolved inorganic carbon increase of approximately 0.55 μmol kg⁻¹. These anthropogenic CO₂ levels would not be detectable using current coulometric techniques (precision of approximately ± 2 μmol kg⁻¹) to measure dissolved inorganic carbon but are easily detectable using CFCs. Assuming a mean Samoan Passage transport of 8 Sv (Roemmich et al. 1996) and integrating over time indicates that a total of 0.1 Pg of anthropogenic carbon had passed through the Samoan Passage by 2009, 20% of which had transited the Samoan Passage before 1900. Although this is a small amount, the anthropogenic carbon transport will increase and represents CO₂ sequestered on centennial and longer timescales.

5. WARMING, FRESHENING, AND A DECLINE IN VENTILATION OF ANTARCTIC BOTTOM WATER

The above studies have all assumed a steady-state deep circulation. However, revisiting the WOCE sections during CLIVAR and GO-SHIP has revealed a global-scale warming of AABW, implying significant changes to the deep ventilation of AABW (Purkey & Johnson 2010) (**Figure 7**). Compiled with growing evidence of anthropogenic and natural variability at and near formation sites, this warming has been linked to a possible slowdown of the bottom limb of the MOC (Masuda et al. 2010). The exact mechanisms driving these changes are still poorly understood, however.

A useful framework for evaluating abyssal variability along repeated hydrographic sections is to distinguish deep changes caused by a change in the water mass properties (water mass change) from changes in isopycnal depths (isopycnal heave) (Bindoff & McDougall 1994, Purkey & Johnson 2013). A large-scale rising or falling of isopycnals within a deep interior water mass reflects a change in the volume and could be associated with a shift in the ventilation. Alternatively, a water mass freshening or warming could reflect a change in one or more of the water mass end members and represent change advected from its source region.

The AABW in the Atlantic and Indo-Pacific sectors of the Southern Ocean have experienced different trends over the past three decades and are discussed separately below. AABW in the Atlantic sector has reduced in volume with little or no water mass freshening (Purkey & Johnson 2012, 2013) (**Figure 7**). AABW in the Indo-Pacific sector has freshened following a 0.03 decade⁻¹ freshening of the Ross Shelf waters since the 1950s (Jacobs 2002, Jacobs & Giulivi 2010). Oxygen and CFC data from both sectors, however, suggest that the ventilation is slowing down in both oceans (Huhn et al. 2013).

5.1. Antarctic Bottom Water Warming in the Atlantic

Early evidence of variability in the bottom limb of the MOC started to emerge in the early 1990s in deep regions of the Atlantic ventilated by WSBW. Closest to the source, WSBW within the Weddell Gyre warmed by approximately 0.02°C between 1990 and 2005, associated with a loss in WSBW volume (Fahrback et al. 2004, 2011; Purkey & Johnson 2010). On isobars, WSDW warmed and became more saline between the 1980s and 2000s (Robertson et al. 2002, Fahrback et al. 2004, Meredith et al. 2014). However, Purkey & Johnson (2012) showed that this warming

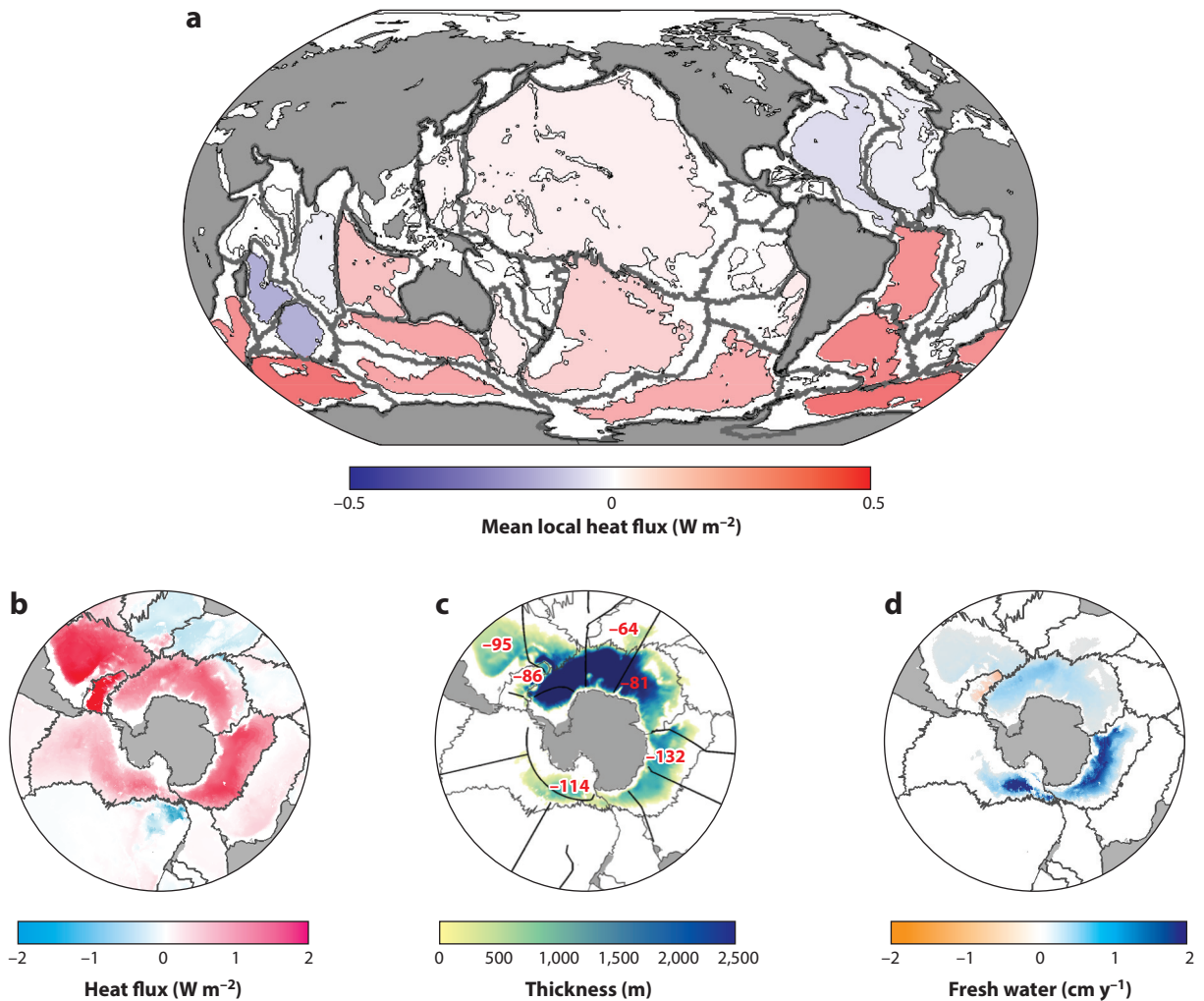


Figure 7

(a) Global map of the mean local heat flux through the 4,000-m isobath needed to account for the deep warming trend in each deep basin (*gray lines*) using all repeated hydrographic sections from 1981 through 2015. (b–d) Polar projections showing the warming caused by heave (panel b) and freshening caused by water mass shifts (panel d), along with displacement of the 0°C isotherm (*red numbers*) plotted over mean thickness of the 0°C isotherm (panel c). Panel a adapted from Desbruyères et al. (2016). Panels b and d adapted from Purkey & Johnson (2013) with permission; copyright American Meteorological Society. Panel c adapted from Johnson & Purkey (2013), based on Purkey & Johnson (2012).

and salinification of WSDW was due to isopycnal heave as part of the volume retraction of WSBW and indicated no property or volume change in WSDW.

Furthermore, repeated transient tracer sections across the Weddell Sea from 1984 to 2011 revealed an increase in the tracer age of the deep and bottom waters (Huhn et al. 2013). Huhn et al. (2013) used the TTD method to calculate the mean tracer age of deep and bottom water along the 10 occupations of the prime meridian section and six occupations of the WOCE S04 section (roughly zonal along 65°S) across the Weddell Sea. This remarkably well-resolved 27-year

time series clearly showed a 15–21% decline in the ventilation rate over the time period, with a linear increase in the mean age of the bottom water.

AABW in the deep western south Atlantic basins, fed by WSDW and WSBW, has shown more variability in its warming trend (Johnson & Doney 2006, Meredith et al. 2008, Johnson et al. 2014). Coles et al. (1996) used historical data from the 1980s to demonstrate that the density and volume of AABW in the Argentine Basin had declined. Johnson & Doney (2006) showed a continuing of this trend with warming on isobars of $0.04^{\circ}\text{C decade}^{-1}$ along the A16S line through 2005 not only in the Argentine Basin but also in the Brazil Basin and Scotia Sea. However, Johnson et al. (2014) found more variability across the two southernmost basins during the most recent 2014 occupation, with cooling in parts of the deep Scotia Sea and Argentine Basin. The best-sampled deep time series is near the northern extent of AABW in the Atlantic in the Vema Channel, between the Argentine and Brazil Basins. Using data collected from 1970 to 2010, Zenk & Morozov (2007) and Zenk & Visbeck (2013) showed that the AABW in this area has warmed steadily at a rate of $0.028^{\circ}\text{C decade}^{-1}$. In addition to the warming, an observable water mass freshening might be under way in the Scotia Sea owing to increased glacial melt from the Antarctic Peninsula; however, the freshening is still small and close to the detection limit (Jullion et al. 2013, Meredith et al. 2014).

Studies using all repeated hydrographic sections from 1980 to 2010 in the Atlantic confirm that the strongest deep warming trends are in the Weddell Sea, with slightly slower warming rates to the north in the deep (below 4,000 m) western Atlantic basins fed by AABW (Purkey & Johnson 2010, Kouketsu et al. 2011) (**Figure 7a**). Using an additional five years of data, Desbruyères et al. (2016) showed that this warming continues but at a slower rate with less statistical significance, indicating a possible slowdown of the Atlantic warming pattern between the 2000s and 2010s.

The western Atlantic deep warming was forced by a deep negative isopycnal heave, suggesting that this warming was caused by a decrease in the volume of WSBW, driving decreased ventilation to the north (Purkey & Johnson 2012) (**Figure 7a,c**). Kouketsu et al. (2011) suggested that there has been a reduction of the northward-flowing abyssal water across 35°S of 0.4 Sv, supporting this conclusion. However, although a simple conceptual model in which a reduced WSBW forces an isopycnal heave warming signal throughout the western Atlantic is plausible, the direct connection between the variability in the WSBW and deep warming to the north is still not clear. Data from mooring arrays between the Weddell Sea and the Scotia Sea suggest a wind-driven connection between the basins (Gordon et al. 2010; Jullion et al. 2010; McKee et al. 2011; Meredith et al. 2011, 2014). This work suggests that as the Weddell Gyre spins up or down, the isopycnals will dome more or less, changing the density of overflow waters and the bottom limb of the Atlantic MOC to the north (see Section 2). Therefore, both bottom water formation rates and the surface winds and position of the Antarctic Circumpolar Current could influence the bottom water properties to the north.

5.2. Indo-Pacific Warming and Freshening

In contrast to the Atlantic, a continuous strong water mass freshening trend has dominated the changes in AABW in the Southern Ocean Indo-Pacific deep basins. This freshening has been tied to the 0.03 decade^{-1} freshening of the HSSW and ISW end members on the Ross Shelf from the 1950s to the present, possibly because of increased glacial melting in West Antarctica (Jacobs 2002, Jacobs & Giulivi 2010). Near Cape Adare directly downstream, AABW freshening has been observed both in repeated hydrographic sections and in moorings (Swift & Orsi 2012, Gordon et al. 2015), with some evidence of decreased ventilation (Rivaro et al. 2010), although the temporal data coverage of these sections is poor relative to the high-frequency variability typical in

this region. The abyssal plain of the Australian-Antarctic Basin has also freshened throughout the basin, with AABW salinity decreasing by as much as 0.06 PSU between the 1970s and 2010s close to the east end of the basin (Aoki et al. 2005, Johnson et al. 2008, Purkey & Johnson 2013, van Wijk & Rintoul 2014, Menezes et al. 2017) (**Figure 7d**). The deep freshening of the Australian-Antarctic Basin could be caused by recent freshening of RSBW, which flows into the basin from the Pacific (e.g., Jacobs 2002, Purkey & Johnson 2013), or a decrease in the volume of RSBW and increase in local Adélie Land Bottom Water, which is fresher than RSBW (van Wijk & Rintoul 2014, Menezes et al. 2017). Together, the observed freshening in the Ross Sea and Australian-Antarctic Basin is equivalent to a flux of 73 gigatons y^{-1} (0.032 Sv) of fresh water into AABW between the mid-1990s and mid-2000s (Purkey & Johnson 2013) (**Figure 7d**).

Even more striking, north of the Southern Ocean, AABW warmed uniformly in the East Indian Ocean and throughout the Pacific deep basins between the 1990s and 2010s (Fukasawa et al. 2004, Kawano et al. 2006, Johnson et al. 2007, Masuda et al. 2010, Purkey & Johnson 2010, Kouketsu et al. 2011) (**Figure 7a**), with no statistically significant change in the warming rate over these three decades (Desbruyères et al. 2016). This global-scale warming signal has been attributed to a decrease in AABW production communicated throughout the Indo-Pacific through a thermocline readjustment via Kelvin and Rossby waves on decadal timescales (Masuda et al. 2010). The warming is driven by isotherm heave, reflecting a decline in northward transport of AABW across 24°N in the Pacific (Kouketsu et al. 2009).

Finally, oxygen and CFCs on repeated hydrographic sections near AABW source regions indicate a decline in RSBW ventilation in the Ross Sea and Australian-Antarctic Basin (Ozaki et al. 2009; Katsumata et al. 2015; S.G. Purkey, W.M. Smethie Jr. & S.S. Jacobs, manuscript in preparation). In the Ross Sea, oxygen levels have fallen in AABW, indicating a decrease in local AABW production (Ozaki et al. 2009). In addition, CFC-11 data from 1992 and SF₆ data from 2011 occupations of line S4P across the Ross Sea at 64°S revealed that the mean tracer age of the AABW shelf water component was 5–10 years greater in 2011 than it was in 1992 (S.G. Purkey, W.M. Smethie Jr. & S.S. Jacobs, manuscript in preparation). In the Australian-Antarctic Basin, oxygen, salinity, and temperature data suggest more influence from Adélie Land Bottom Water and less from RSBW in the coastal current and deep basin, again suggesting a decrease in the production of RSBW (Ozaki et al. 2009, Katsumata et al. 2015).

6. CONCLUSION

Compared with North Atlantic Deep Water, AABW has been undersampled in time and space owing to the Southern Ocean's harsh conditions, enormous size, and remoteness. Nonetheless, the limited tracer data available have allowed for assessment of the formation and circulation of AABW within the Southern Ocean and around the world.

As more tracer data have become available, they have confirmed that the bottom limb of the MOC has had a high degree of variability over the past four decades. AABW has warmed around the globe, likely tied to a decrease in ventilation and a slowdown in AABW production. This warming adds 10% to the total ocean heat storage and increases rates of steric sea level rise by 8% (Purkey & Johnson 2010). However, the exact mechanisms driving the abyssal warming are still poorly understood. In addition, how a global-scale slowdown of the AABW cell of the MOC will affect ocean carbon storage and uptake is still unknown (Arrigo et al. 2008). The use of transient tracers to evaluate these changes in AABW is just beginning (Huhn et al. 2013; S.G. Purkey, W.M. Smethie Jr. & S.S. Jacobs, manuscript in preparation) and will be a key tool in advancing our understanding of AABW variability and how this variability will feed back on the climate system.

DISCLOSURE STATEMENT

The authors are not aware of any affiliations, memberships, funding, or financial holdings that might be perceived as affecting the objectivity of this review.

ACKNOWLEDGMENTS

We thank Breck Owens for support with the analysis and mapping of the GLODAPv2 data presented in **Figure 5**. S.G.P. was supported by National Science Foundation (NSF) grants OCE-1060804 and OCE-1437015. A.L.G.'s contribution was funded by the National Oceanic and Atmospheric Administration (NOAA) Climate Observation Division, US Department of Commerce, via grant UCAR Z15-17551. G.G. was supported by NSF grants OCE-1357121 and OCE-1536380. J.L.B. was supported by the NOAA Climate Observation Division. R.E.S. and M.J.W. were supported by NSF grant OCE-0762517. M.J.W.'s contribution was funded by NSF grants OCE-1536115 and OCE-0726517 for tracer measurements along P15S. NSF grant OPP04-40825 supported the collection of the CFC measurements presented in **Figure 4**. Data used throughout this review were collected, calibrated, and made available through the GO-SHIP program. The statements, findings, conclusions, and recommendations are those of the authors and do not necessarily reflect the views of NOAA or the Department of Commerce. This article is Lamont-Doherty Earth Observatory contribution number 8119 and NOAA Pacific Marine Environmental Laboratory publication 4658.

LITERATURE CITED

- Aoki S, Rintoul SR, Ushio S, Watanabe S, Bindoff NL. 2005. Freshening of the Adélie Land bottom water near 140°E. *Geophys. Res. Lett.* 32:L23601
- Arrigo KR, van Dijken G, Long M. 2008. Coastal Southern Ocean: a strong anthropogenic CO₂ sink. *Geophys. Res. Lett.* 35:L21602
- Baines PG, Condie S. 1998. Observations and modelling of Antarctic downslope flows: a review. See Jacobs & Weiss 1998, pp. 29–49
- Bindoff NL, McDougall TJ. 1994. Diagnosing climate change and ocean ventilation using hydrographic data. *J. Phys. Oceanogr.* 24:1137–52
- Bretherton FP, Davis RE, Fandry CB. 1976. A technique for objective analysis and design of oceanographic experiments applied to MODE-73. *Deep-Sea Res. Oceanogr. Abstr.* 23:559–82
- Broecker WS, Peng T. 1982. *Tracers in the Sea*. Palisades, NY: Lamont-Doherty Geol. Obs.
- Bullister JL. 1989. Chlorofluorocarbons as time dependent tracers in the ocean. *Oceanography* 2(2):12–17
- Bullister JL. 2015. *Atmospheric Histories 1765–2015 for CFC-11, CFC-12, CFC-113, CCl₄, SF₆ and N₂O*. NDP-095, Carbon Dioxide Inf. Anal. Cent., Oak Ridge Natl. Lab., US Dep. Energy, Oak Ridge, Tenn. https://www.nodc.noaa.gov/ocads/oceans/CFC_ATM_Hist2015.html
- Bullister JL, Weiss RF. 1983. Anthropogenic chlorofluoromethanes in the Greenland and Norwegian Seas. *Science* 221:265–68
- Cheon WG, Lee SK, Gordon AL, Liu Y, Cho CB, Park JJ. 2015. Replicating the 1970s' Weddell Polynya using a coupled ocean-sea ice model with reanalysis surface flux fields. *Geophys. Res. Lett.* 42:5411–18
- Coles VJ, McCartney MS, Olson DB, Smethie WM Jr. 1996. Changes in Antarctic Bottom Water properties in the western South Atlantic in the late 1980s. *J. Geophys. Res.* 101:8957–70
- Desbruyères DG, Purkey SG, McDonagh EL, Johnson GC, King BA. 2016. Deep and abyssal ocean warming from 35 years of repeat hydrography. *Geophys. Res. Lett.* 43:10356–65
- Doney SC, Bullister JL. 1992. A chlorofluorocarbon section in the eastern North Atlantic. *Deep-Sea Res. A* 39:1857–83
- Doney SC, Jenkins WJ. 1994. Ventilation of the deep western boundary current and abyssal western North Atlantic: estimates from tritium and ³He distributions. *J. Phys. Oceanogr.* 24:638–59

- Fahrbach E, Hoppema M, Rohardt G, Boebel O, Klatt O, Wisotzki A. 2011. Warming of deep and abyssal water masses along the Greenwich meridian on decadal time scales: the Weddell gyre as a heat buffer. *Deep-Sea Res. II* 58:2509–23
- Fahrbach E, Hoppema M, Rohardt G, Schroder M, Wisotzki A. 2004. Decadal-scale variations of water mass properties in the deep Weddell Sea. *Ocean Dyn.* 54:77–91
- Fahrbach E, Rohardt G, Scheele N, Schröder M, Strass V, Wisotzki A. 1995. Formation and discharge of deep and bottom water in the northwestern Weddell Sea. *J. Mar. Res.* 53:515–38
- Fine RA, Molinari RL. 1988. A continuous deep western boundary current between Abaco (26.5°N) and Barbados (13°N). *Deep-Sea Res. A* 35:1441–50
- Fine RA, Rhein M, Andrie C. 2003. Using a CFC effective age to estimate propagation and storage of climate anomalies in the deep western North Atlantic Ocean. *Geophys. Res. Lett.* 29:2227
- Foster TD, Carmack EC. 1976. Frontal zone mixing and Antarctic Bottom Water formation in the southern Weddell Sea. *Deep-Sea Res. Oceanogr. Abstr.* 23:301–17
- Fukasawa M, Freeland H, Perkin R, Watanabe T. 2004. Bottom water warming in the North Pacific Ocean. *Nature* 427:825–27
- Gebbie G, Huybers P. 2011. How is the ocean filled? *Geophys. Res. Lett.* 38:L06604
- Gordon AL. 1966. Potential temperature, oxygen and circulation of bottom water in the Southern Ocean. *Deep-Sea Res. Oceanogr. Abstr.* 13:1125–38
- Gordon AL. 1974. Varieties and variability of Antarctic Bottom Water. In *Processus de Formation des Eaux Oceaniques Profondes en Particulier en Mediterranee Occidentale*, pp. 33–47. Paris: CNRS
- Gordon AL. 1978. Deep Antarctic convection west of Maud Rise. *J. Phys. Oceanogr.* 8:600–12
- Gordon AL. 1998. Western Weddell Sea thermohaline stratification. See Jacobs & Weiss 1998, pp. 215–40
- Gordon AL. 2013. Bottom water formation. In *Encyclopedia of Ocean Sciences*, ed. JH Steele, KK Turekian, SA Thorpe, pp. 415–21. San Diego, CA: Academic. 2nd ed. <https://doi.org/10.1016/B978-0-12-409548-9.04019-7>
- Gordon AL. 2014. Oceanography: Southern Ocean polynya. *Nat. Clim. Change* 4:249–50
- Gordon AL, Huber BA, Busecke J. 2015. Bottom water export from the western Ross Sea, 2007 through 2010. *Geophys. Res. Lett.* 42:5387–94
- Gordon AL, Huber BA, Hellmer H, Ffield A. 1993. Deep and Bottom Water of the Weddell Sea's western rim. *Science* 262:95–97
- Gordon AL, Huber BA, McKee D, Visbeck MH. 2010. A seasonal cycle in the export of bottom water from the Weddell Sea. *Nat. Geosci.* 3:551–56
- Gordon AL, Orsi AH, Muench R, Huber BA, Zambianchi E, Visbeck M. 2009. Western Ross Sea continental slope gravity currents. *Deep-Sea Res. II* 56:796–817
- Gordon AL, Tchernia P. 1972. Waters of the continental margin off Adélie Coast, Antarctica. In *Antarctica Oceanology II: The Australian-New Zealand Sector*, ed. DE Hayes, pp. 59–69. Antarct. Res. Ser. Vol. 19. Washington, DC: Am. Geophys. Union
- Gordon AL, Visbeck M, Comiso JC. 2007. A possible link between the Weddell Polynya and the Southern Annular Mode. *J. Clim.* 20:2558–71
- Gordon AL, Zambianchi E, Orsi A, Visbeck M, Giulivi CF, et al. 2004. Energetic plumes over the western Ross Sea continental slope. *Geophys. Res. Lett.* 31:L21302
- Gouretski VV, Koltermann KP. 2004. *WOCE global hydrographic climatology*. Tech. Rep. 35, Ber. Bundesamtes Seeschiffahrt Hydrogr., Hamburg, Ger.
- Haine TW, Watson AJ, Liddicoat MI, Dickson RR. 1998. The flow of Antarctic bottom water to the southwest Indian Ocean estimated using CFCs. *J. Geophys. Res.* 103:27637–53
- Heywood KJ, Schmidt S, Heuzé C, Kaiser J, Jickells TD, et al. 2014. Ocean processes at the Antarctic continental slope. *Philos. Trans. R. Soc. A* 372:20130047
- Holzer M, Primeau FW, Smethie WM Jr., Khatiwala S. 2010. Where and how long ago was water in the western North Atlantic ventilated? Maximum entropy inversions of bottle data from WOCE line A20. *J. Geophys. Res.* 115:C07005
- Huhn O, Hellmer HH, Rhein M, Rodehacke C, Roether W, et al. 2008. Evidence of deep- and bottom-water formation in the western Weddell Sea. *Deep-Sea Res. II* 55:1098–116

- Huhn O, Rhein M, Hoppema M, van Heuven S. 2013. Decline of deep and bottom water ventilation and slowing down of anthropogenic carbon storage in the Weddell Sea 1984–2011. *Deep-Sea Res. I* 76:66–84
- Jacobs SS. 2002. Freshening of the Ross Sea during the late 20th century. *Science* 297:386–89
- Jacobs SS. 2004. Bottom water production and its links with the thermohaline circulation. *Antarct. Sci.* 164:427–37
- Jacobs SS, Amos AF, Bruchhausen PM. 1970. Ross Sea oceanography and Antarctic Bottom Water formation. *Deep-Sea Res. Oceanogr. Abstr.* 176:935–62
- Jacobs SS, Comiso JC. 1989. Sea ice and oceanic processes on the Ross Sea continental shelf. *J. Geophys. Res.* 94:18195–211
- Jacobs SS, Fairbanks RG, Horibe Y. 1985. Origin and evolution of water masses near the Antarctic continental margin: evidence from $H_2^{18}O/H_2^{16}O$ ratio in seawater. In *Oceanology of the Antarctic Continental Shelf*, ed. SS Jacobs, pp. 59–85. Antarct. Res. Ser. Vol. 43. Washington, DC: Am. Geophys. Union
- Jacobs SS, Giulivi CF. 2010. Large multidecadal salinity trends near the Pacific–Antarctic continental margin. *J. Clim.* 2317:4508–24
- Jacobs SS, Weiss RF, eds. 1998. *Ocean, Ice, and Atmosphere: Interactions at the Antarctic Continental Margin*. Antarct. Res. Ser. Vol. 75. Washington, DC: Am. Geophys. Union
- Johnson GC, Doney SC. 2006. Recent western South Atlantic bottom water warming. *J. Geophys. Res.* 33:L14614
- Johnson GC, McTaggart KE, Wanninkhof R. 2014. Antarctic Bottom Water temperature changes in the western South Atlantic from 1989–2014. *J. Geophys. Res.* 119:8567–77
- Johnson GC, Mecking S, Sloyan BM, Wijffels SE. 2007. Recent bottom water warming in the Pacific Ocean. *J. Clim.* 20:5365–75
- Johnson GC, Purkey SG. 2013. Slowdown of the lower, southern limb of the meridional overturning circulation in recent decades. *Bull. Am. Meteorol. Soc.* 94:S68–69
- Johnson GC, Purkey SG, Bullister JL. 2008. Warming and freshening in the abyssal southeastern Indian Ocean. *J. Clim.* 21:5351–63
- Jullion L, Jones SC, Naveira Garabato AC, Meredith MP. 2010. Wind-controlled export of Antarctic Bottom Water from the Weddell Sea. *Geophys. Res. Lett.* 379:L09609
- Jullion L, Naveira Garabato AC, Meredith MP, Holland PR, Courtois P, King BA. 2013. Decadal freshening of the Antarctic Bottom Water exported from the Weddell Sea. *J. Clim.* 26:8111–25
- Katsumata K, Nakano H, Kumamoto Y. 2015. Dissolved oxygen change and freshening of Antarctic Bottom Water along 62°S in the Australian–Antarctic Basin between 1995/1996 and 2012/2013. *Deep-Sea Res. II* 114:27–38
- Kawano T, Fukasawa M, Kouketsu S, Uchida H, Doi T, et al. 2006. Bottom water warming along the pathway of Lower Circumpolar Deep Water in the Pacific Ocean. *Geophys. Res. Lett.* 3323:L23613
- Klatt O, Roether W, Hoppema M, Bulsiewicz K, Fleischmann U, et al. 2002. Repeated CFC sections at the Greenwich Meridian in the Weddell Sea. *J. Geophys. Res.* 107:3030
- Kouketsu S, Doi T, Kawano T, Masuda S, Sugiura N, et al. 2011. Deep ocean heat content changes estimated from observation and reanalysis product and their influence on sea level change. *J. Geophys. Res.* 116:C03012
- Kouketsu S, Fukasawa M, Kaneko I, Kawano T, Uchida H, et al. 2009. Changes in water properties and transports along 24°N in the North Pacific between 1985 and 2005. *J. Geophys. Res.* 114:C01008
- LeBel DA, Smethie WM Jr., Rhein M, Kieke D, Fine RA, et al. 2008. The distribution of CFC-11 in the North Atlantic during WOCE: inventories and calculated water mass formation rates. *Deep-Sea Res. I* 55:891–910
- Legg S, Briegleb B, Chang Y, Chassignet E, Danabasoglu G, et al. 2009. Improving oceanic overflow representation in climate models: the Gravity Current Entrainment Climate Process Team. *Bull. Am. Meteorol. Soc.* 905:657–70
- Loose B, Schlosser P, Smethie WM Jr., Jacobs S. 2009. An optimized estimate of glacial melt from the Ross Ice Shelf using noble gases, stable isotopes, and CFC transient tracers. *J. Geophys. Res.* 114:C08007
- Masuda S, Awaji T, Sugiura N, Matthews JP, Toyoda T, et al. 2010. Simulated rapid warming of abyssal North Pacific waters. *Science* 329:319–22

- McKee D, Yuan X, Gordon AL, Huber BA, Dong Z. 2011. Climate impact on interannual variability of Weddell Sea Bottom Water. *J. Geophys. Res.* 116:C05020
- Menezes VV, Macdonald AM, Schatzman C. 2017. Accelerated freshening of Antarctic Bottom Water over the last decade in the Southern Indian Ocean. *Sci. Adv.* 31:e1601426
- Mensch M, Bayer R, Bullister JL, Schlosser P, Weis RF. 1996. The distribution of tritium and CFCs in the Weddell Sea during the mid-1980s. *Prog. Oceanogr.* 38:377–415
- Meredith MP, Gordon AL, Naveira Garabato AC, Abrahamsen EP, Huber BA, et al. 2011. Synchronous intensification and warming of Antarctic Bottom Water outflow from the Weddell Gyre. *Geophys. Res. Lett.* 38:L03603
- Meredith MP, Jullion L, Brown PJ, Naveira Garabato AC, Couldrey MP. 2014. Dense waters of the Weddell and Scotia Seas: recent changes in properties and circulation. *Philos. Trans. R. Soc. A* 372:20130041
- Meredith MP, Naveira Garabato AC, Gordon A, Johnson GC. 2008. Evolution of the Deep and Bottom Waters of the Scotia Sea, Southern Ocean, during 1995–2005. *J. Clim.* 21:3327–43
- Meredith MP, Watson AJ, Van Scoy K, Haine TWN. 2001. Chlorofluorocarbon-derived formation rates of the deep and bottom waters of the Weddell Sea. *J. Geophys. Res.* 106:2899–919
- Nihashi S, Ohshima KI. 2015. Circumpolar mapping of Antarctic coastal polynyas and landfast sea ice: relationship and variability. *J. Clim.* 28:3650–70
- Ohshima KI, Fukamachi Y, Williams GD, Nihashi S, Roquet F, et al. 2013. Antarctic Bottom Water production by intense sea-ice formation in the Cape Darnley Polynya. *Nat. Geosci.* 6:235–40
- Olsen A, Key R, van Heuven S, Lauvset SK, Velo A, et al. 2016. The Global Ocean Data Analysis Project version 2 (GLODAPv2)—an internally consistent data product for the world ocean. *Earth Syst. Sci. Data* 8:297–323
- Orsi AH, Jacobs SS, Gordon AL, Visbeck M. 2001. Cooling and ventilating the abyssal ocean. *Geophys. Res. Lett.* 28:2923–26
- Orsi AH, Johnson GC, Bullister JL. 1999. Circulation, mixing, and production of Antarctic Bottom Water. *Prog. Oceanogr.* 43:1:55–109
- Orsi AH, Smethie WM Jr., Bullister JL. 2002. On the total input of Antarctic waters to the deep ocean: a preliminary estimate from chlorofluorocarbon measurements. *J. Geophys. Res.* 107:31–1–14
- Orsi AH, Wiederwohl CL. 2009. A recount of Ross Sea waters. *Deep-Sea Res. II* 56:778–95
- Ozaki H, Obata H, Naganobu M, Gamo T. 2009. Long-term bottom water warming in the north Ross Sea. *J. Oceanogr.* 65:235–44
- Paul S, Willmes S, Heinemann G. 2015. Long-term polynya dynamics in the southern Weddell Sea from MODIS thermal-infrared imagery. *Cryosphere* 9:2027–41
- Pickart RS, Hogg NG, Smethie WM Jr. 1989. Determining the strength of the deep western boundary current using the chlorofluoromethane ratio. *J. Phys. Oceanogr.* 19:940–51
- Purkey SG, Johnson GC. 2010. Warming of global abyssal and deep Southern Ocean waters between the 1990s and 2000s: contributions to global heat and sea level rise budgets. *J. Clim.* 23:6336–51
- Purkey SG, Johnson GC. 2012. Global contraction of Antarctic Bottom Water between the 1980s and 2000s. *J. Clim.* 25:5830–44
- Purkey SG, Johnson GC. 2013. Antarctic Bottom Water warming and freshening: contributions to sea level rise, ocean freshwater budgets, and global heat gain. *J. Clim.* 26:6105–22
- Rhein M, Fischer J, Smethie WM Jr., Smythe-Wright D, Weiss RF, et al. 2002. Labrador Sea Water: pathways, CFC inventory and formation rates. *J. Phys. Oceanogr.* 32:648–65
- Rhein M, Stramma L, Krahnmann G. 1998. The spreading of Antarctic bottom water in the tropical Atlantic. *Deep-Sea Res. I* 45:507–27
- Rintoul SR. 1998. On the origin and influence of Adélie Land bottom water. See Jacobs & Weiss 2013, pp. 151–71
- Rivaro P, Massolo S, Bergamasco A, Castagno P, Budillon G. 2010. Chemical evidence of the changes of the Antarctic Bottom Water ventilation in the western Ross Sea between 1997 and 2003. *Deep-Sea Res. I* 57:639–52
- Robertson R, Visbeck M, Gordon AL. 2002. Long-term temperature trends in the deep waters of the Weddell Sea. *Deep-Sea Res. II* 49:4791–806

- Rodehacke CB, Roether W, Hellmer H, Hall T. 2009. Temporal variations and trends of CFC11 and CFC12 surface-water saturations in Antarctic marginal seas: results of a regional ocean circulation model. *Deep-Sea Res. I* 57:175–98
- Roemmich D, Hautala S, Rudnick D. 1996. Northward abyssal transport through the Samoan Passage and adjacent regions. *J. Geophys. Res.* 101:14039–55
- Schlosser P. 1986. Helium: a new tracer in Antarctic oceanography. *Nature* 321:233–35
- Schlosser P, Bayer R, Foldvik A, Gammelsrød T, Rohardt G, Münnich KO. 1990. Oxygen 18 and helium as tracers of ice shelf water and water/ice interaction in the Weddell Sea. *J. Geophys. Res.* 95:3253–63
- Schlosser P, Bullister JL, Bayer R. 1991. Studies of deep water formation and circulation in the Weddell Sea using natural and anthropogenic tracers. *Mar. Chem.* 35:97–122
- Smethie WM Jr. 1993. Tracing the thermohaline circulation in the western North Atlantic, using chlorofluorocarbons. *Prog. Oceanogr.* 31:51–99
- Smethie WM Jr., Fine RA. 2001. Rates of North Atlantic Deep Water formation calculated from chlorofluorocarbon inventories. *Deep-Sea Res. I* 48:189–215
- Smethie WM Jr., Fine RA, Putzka A, Jones EP. 2000. Tracing the flow of North Atlantic Deep Water using chlorofluorocarbons. *J. Geophys. Res.* 105:14299–323
- Smethie WM Jr., Jacobs SS. 2005. Circulation and melting under the Ross Ice Shelf: estimates from evolving CFC, salinity and temperature fields in the Ross Sea. *Deep-Sea Res. I* 52:959–78
- Steinfeldt RM, Rhein M, Bullister JL, Tanhua T. 2009. Inventory changes in anthropogenic carbon from 1997–2003 in the Atlantic Ocean between 20°S and 65°N. *Glob. Biogeochem. Cycles* 23:GB3010
- Stewart AL, Thompson AF. 2012. Sensitivity of the ocean's deep overturning circulation to easterly Antarctic winds. *Geophys. Res. Lett.* 39:L18604
- Stewart AL, Thompson AF. 2013. Connecting Antarctic cross-slope exchange with Southern Ocean overturning. *J. Phys. Oceanogr.* 43:1453–71
- Stewart AL, Thompson AF. 2015. Eddy-mediated transport of warm Circumpolar Deep Water across the Antarctic Shelf Break. *Geophys. Res. Lett.* 42:432–40
- Sverdrup HU, Johnson MW, Fleming RH. 1942. *The Oceans: Their Physics, Chemistry, and General Biology*. New York: Prentice-Hall. <http://ark.cdlib.org/ark:/13030/kt167nb66r>
- Swift J, Orsi AH. 2012. Sixty-four days of hydrography and storms: RVIB *Nathaniel B. Palmer's* 2011 S04P Cruise. *Oceanography* 25(3):54–55
- Talley LD, Feely RA, Sloyan BM, Wanninkhof R, Baringer MO, et al. 2016. Changes in ocean heat, carbon content, and ventilation: a review of the first decade of GO-SHIP global repeat hydrography. *Annu. Rev. Mar. Sci.* 8:185–215
- Trumbore SE, Jacobs SS, Smethie WM Jr. 1991. Chloro-fluorocarbon evidence for rapid ventilation of the Ross Sea. *Deep-Sea Res.* 38:845–70
- Van Sebille E, Spence P, Mazloff MR, England MH, Rintoul SS, Saenko OA. 2013. Abyssal connections of Antarctic Bottom Water in a Southern Ocean state estimate. *Geophys. Res. Lett.* 40:2177–82
- van Wijk EM, Rintoul SS. 2014. Freshening drives contraction of Antarctic Bottom Water in the Australian Antarctic Basin. *Geophys. Res. Lett.* 41:1657–64
- Wang Z, Wu Y, Lin X, Liu C, Xie Z. 2017. Impacts of open ocean deep convection in the Weddell Sea on coastal and bottom water temperature. *Clim. Dyn.* 48:2967–81
- Warner MJ, Weiss RF. 1985. Solubilities of chlorofluorocarbons 11 and 12 in water and seawater. *Deep-Sea Res. II* 32:1485–97
- Waugh DW, Haine TWN, Hall TM. 2004. Transport times and anthropogenic carbon in the subpolar North Atlantic Ocean. *Deep-Sea Res. I* 51:1475–91
- Waugh DW, Hall TM. 2005. Propagation of tracer signals in boundary currents. *J. Phys. Oceanogr.* 35:1538–52
- Weiss RF, Bullister JL, Gammon RH, Warner MJ. 1985. Atmospheric chlorofluoromethanes in the deep equatorial Atlantic. *Nature* 314:608–10
- Weiss RF, Ostlund HG, Craig H. 1979. Geochemical studies of the Weddell Sea. *Deep-Sea Res. A* 26:1093–120
- Weppernig R, Schlosser P, Khatiwala S, Fairbanks RG. 1996. Isotope data from Ice Station Weddell: implications for deep water formation in the Weddell Sea. *J. Geophys. Res.* 101:25723–39
- Williams GD, Aoki S, Jacobs SS, Rintoul SR, Tamura T, Bindoff NL. 2010. Antarctic Bottom Water from the Adélie and George V Land coast, East Antarctica (140–149°E). *J. Geophys. Res.* 115:C04027

- Williams GD, Bindoff NL, Marsland SJ, Rintoul SR. 2008. Formation and export of dense shelf water from the Adélie Depression, East Antarctica. *J. Geophys. Res.* 113:C04039
- Yabuki T, Suga T, Hanawa K, Matsuoka K, Kiwada H, Watanabe T. 2006. Possible source of the Antarctic Bottom Water in the Prydz Bay region. *J. Oceanogr.* 62:649
- Zenk W, Morozov E. 2007. Decadal warming of the coldest Antarctic Bottom Water flow through the Vema Channel. *Geophys. Res. Lett.* 34:L14607
- Zenk W, Visbeck M. 2013. Structure and evolution of the abyssal jet in the Vema Channel of the South Atlantic. *Deep-Sea Res. II* 85:244–60